The Formation of Galactic Bulges

Ingrid Abraham
Level 4 Project, MPhys Physics and Astronomy
Supervisor: Professor T. Theuns
Department of Physics, Durham University
Submitted: 18/04/2018

This paper presents an investigation of the bulge and disc components of spiral galaxies, and their mechanisms of formation, by way of simulation. Simulation data used in the investigation is from EAGLE project's Ref-L0012N0188 and Ref-L0025N0376 runs of their cosmological hydrodynamical simulation. I present python scripts for classifying galaxies, decomposing spiral galaxies into bulge and disc components using the angular momentum distribution of their stars, and tracing their histories through the simulation, alongside the results those scripts yield. The formation of galaxies in the simulation was investigated by examining properties of their star particles, such as their age, birth gas density, and element abundances, as well as tracing the kinematics of stars in the galaxies back through their formation. These unanimously support the conclusion that spiral galaxies form "inside out", with the bulge mostly forming first in the early universe, then growing a disc around it by gas accretion. There is also evidence of a lesser process converting disc into bulge, potentially bar formation and destruction. These conclusions are in agreement with recent observational studies of spiral galaxy formation (Margalef-Bentabol et al. 2016).

Contents

1. Introduction 3
A. Outline of Report 3
B. Spiral Galaxy Formation 3
C. The EAGLE Project 5
D. Alpha Enrichment 6

2. Methods 8
A. Accessing the Data 8
B. The Aperture Method 8
C. The Circularity Method 8
1. Finding $L_{\|}$ 9
2. Finding L_c 11
D. Tracing Particles Histories Through the Merger Tree 15

3. Results and Discussion 16
A. The Aperture Method 16
B. The Circularity Method 16
C. Tracing Particle Histories 16
D. Lifetime Changes 22
E. Further Work 23

4. Conclusions 24

Acknowledgments 24

References 25

5. Appendix 27

1. INTRODUCTION

A. Outline of Report

Large galaxies are typically classified in accordance with the Hubble sequence (displayed in Fig. 1) into spheroidal 'elliptical' systems, disc dominated two component 'spiral' systems that consist of a 'disc' which surrounds a central spheroidal 'bulge', and irregularly shaped 'peculiar' galaxies. This paper is primarily concerned with the formation of spiral galaxies and their components, which are investigated using data from the EAGLE (Evolution and Assembly of GaLaxies and their Environments) cosmological hydrodynamical simulations (The EAGLE team 2017a).

I shall begin with a discussion of the background of spiral galaxies and their formation, as well as the EAGLE simulations which I use to investigate them. I will then continue by describing and discussing the methods and approaches used to identify spiral galaxies and their components, as well as to track and analyse them.

In the results section, the findings will be presented, along with a discussion of their implications, and their relevance to real galaxies.

I will conclude with a summary of the results, and a discussion of avenues for future work and further investigation.

B. Spiral Galaxy Formation

The stellar components of spiral galaxies are shown in Fig. 2. The stellar halo is a minor component, containing only a tiny portion of the galaxy's stellar mass, in spherically distributed stars on random orbits. It is generally accepted to be formed from the accretion of dwarf galaxies (E. Bell et al. 2001). The main stellar components are the bulge and disc, whose processes of formation are much more disputed. Morphologically, bulges are spheroidal in shape like small elliptical galaxies, with stellar orbits randomly distributed in direction; discs are disc shaped as the name suggests, with dominantly circular stellar orbits in the plane and direction of the disc's rotation. They are also distinct in colour, with bulges displaying a red colour, while discs typically show as more blue.

The difference in colour reflects a difference in star forming behaviour. The red bulges are dominated by older, redder stellar populations, suggesting little or no new star formation. The blueness of the discs comes from young, short-lived blue stars, suggesting that the disc regions are continually undergoing star formation.

Hubble type galaxies, including spiral galaxies, are the dominant mass component of the galactic population in the local universe. However, the population of Hubble galaxies, especially spiral galaxies, is seen to greatly decrease with increasing redshift, where at high redshift peculiar galaxies dominate (Margalef-Bentabol et al. 2017). This would suggest that the galactic population has undergone severe evolution.

The nature of this evolution remains unknown, and is the subject of many conflicting theories. Some suggest that the bulge forms first in the early universe, and then acquires a disc through gas accretion (Hopkins et al. 2010), others suggest that processes of bar forma-

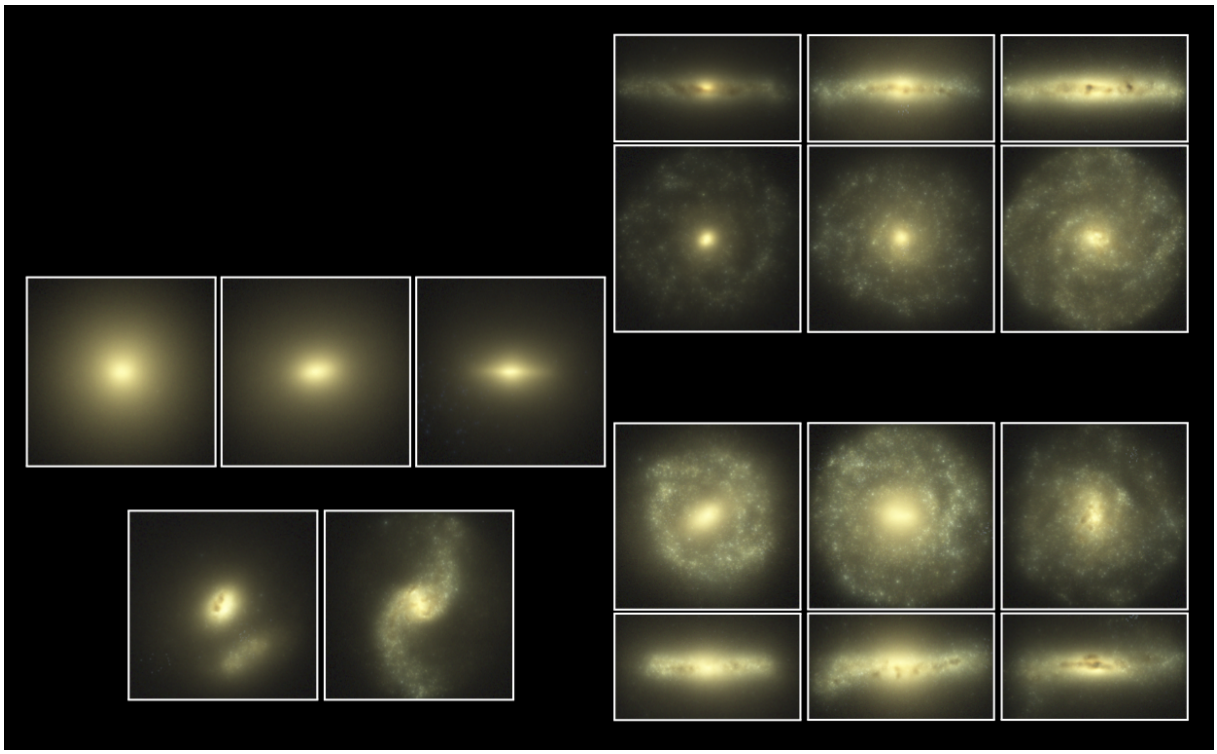

FIG. 1: A "tuning fork" diagram of the Hubble sequence from (The EAGLE team 2017a). The images use galaxies from the EAGLE simulations at z=0.1, rendered using SKIRT software (Verstocken et al. 2017). On the mid left are examples of elliptical galaxies progressing towards lenticular (flattening) as one moves towards the right. On the right are examples of spiral galaxies from both an edge-on and face-on view, with unbarred spirals in the top line, and barred spirals in the bottom line, with spiral arms getting more tightly coiled as one moves towards the right. On the bottom left, outside of the tuning fork, are examples of peculiar galaxies.

tion and destruction convert the central regions of discs into bulges (Sellwood et al. 2004), or that galactic mergers and recent star formation are responsible for bulge and disc formation (Kauffmann et al. 1996).

Current evidence regarding this evolution comes from observational studies such as Margalef-Bentabol et al. 2016, which uses the CANDELS survey (N. Grogin et al. 2011). Such studies broadly conclude that spiral galaxies form "inside-out". That is to say that at high redshift the bulges are already in place, and experience little growth, while the disc later grows around them.

Observational studies have a major limitation, however, which is that they cannot observe the evolution of any given galaxy, since they are limited only to what can currently be observed. Instead, the conclusions are drawn by looking at different galactic populations at different redshifts, and statistically comparing their features.

The aforementioned limitation is addressed in this paper, as data from the EAGLE simulations is used instead of observational data. This enables us to compare galaxies to their progenitors/descendants at different cosmic times, instead of comparing to different galactic populations.

There is, however, a trade-off in using EAGLE. The EAGLE simulations are only simula-

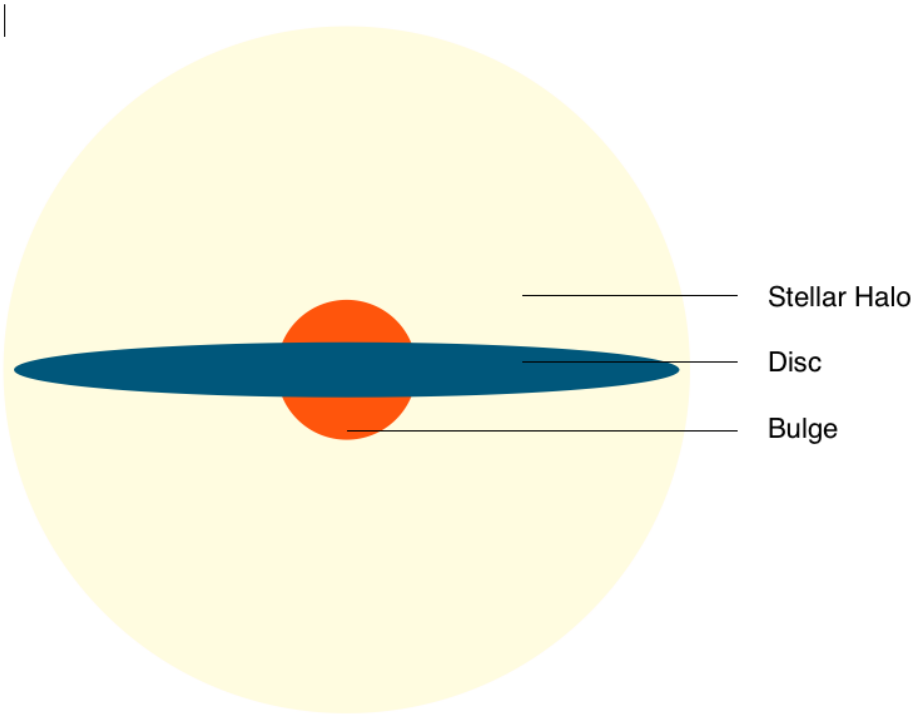

FIG. 2: Edge-on schematic of the stellar components of a spiral galaxy.

tions, and care must be taken when drawing conclusions using them. The simulations are based on our current understanding of physics, and calibrated to reflect observations of the universe, but this is an imperfect process. For work done using EAGLE, one must be careful to consider how well the simulations reflect the real universe, and how details of the simulation may skew results.

C. The EAGLE Project

The EAGLE project is a set of hydrodynamical simulations of cosmologically representative volumes of a ΛCDM universe, from the Virgo Consortium (Schaye et al. 2015). It is primarily intended to look at the formation of galaxies and supermassive black holes.

Simulations in the EAGLE suite are distinguished by volume, in cubes ranging from 12 to 100 Mpc side length, and also in their numerical resolution, and physical calibrations. The simulations were performed using a modification (Schaye et al. 2015) of the Tree SPH code (Springel 2005), so called because of its use of a hierarchical tree, and smoothed particle hydrodynamics.

In this paper, the Ref-L0012N0188 and Ref-L0025N0376 simulations were used, and will hereafter be referred to as the R12 and R25 simulations for brevity. The codenames are a compact description of the simulations, *Ref* indicates that the simulations use the default calibrations (Schaye et al. 2015), while the number after L indicates the side length of the simulation volume in Mpc, and the number after N indicates the cube root of the number of dark matter particles in the simulation (and the initial number of baryonic particles).

Smoothed particle hydrodynamics is a method for computationally simulating fluid dynam-

ics. SPH uses the Lagrangian scheme of fluid dynamics, and works by separating the fluid into 'particles' which move with the fluid flow. There are four kinds of particle, which represent four fluids of the simulation: gas, stars, black holes, and dark matter. These particles are not representative of real-world particles, but are rather relatively large amounts of the fluid, as is necessary for simulations to run in a finite time. An example of this is star particles, which do not contain an individual star or any subdivision thereof, but rather an SSP (simple stellar population), a population of stars that evolve from an initial mass function (O.M. Kurth et al. 1999).

Gas particles in the simulation are 'smoothed' to make the fluid continuous. The particles are given an attribute called smoothing length with units of distance. If a property of the fluid is evaluated at a given point, all particles that have that point within their smoothing length contribute to the evaluation, and their respective contributions are decided by the kernel function. EAGLE uses the C^2 (Wendland 1995) kernel.

The 'Tree' in Tree SPH refers to a hierarchichal tree, or multipole expansion, which is used to index the particles, and simplify computation. This is done using a space-filling Peano-Hilbert curve to fill the volume of the simulation. Particles are indexed according to their location on the curve, allowing neighbouring indices to refer to neighbouring particles. The curve is then divided into subsections called daughter nodes, so that particles far from a given daughter node can perform calculations using only the node instead of all its particles when advancing the time of the simulation, greatly reducing the computational cost.

Processes that occur below the resolution limit in EAGLE are implemented using subgrid models. These include radiative cooling, re-ionisation, star formation, stellar mass loss, type Ia supernovae, energy feedback from star formation, black hole formation, and feedback from AGN.

The EAGLE data is available in two forms, the raw particle data available for download, and an online SQL database of halo and galaxy catalogues, both accessible from the EAGLE project website (The EAGLE team 2017a).

The EAGLE particle data (The EAGLE team 2017b) contains the full specification of the simulation volume at 28 'snapshots', each corresponding to a different cosmic time.

The EAGLE galaxy data (McAlpine et al. 2016) contains data in the same snapshots as the particle data, but instead of particle data, it contains data of halos and galaxies identified using the `FoF` (M. Davis et al. 1985) and `SUBFIND` (K. Dolag et al. 2009) algorithms.

D. Alpha Enrichment

As stars develop, they keep the chemical distribution of the gas they were born from, any changes to this occur only through fusion in the core or accretion. Looking at the chemical makeup of stars can therefore give us an insight into the galaxy at the time of formation of the star, and conversely can be used to date the stars' formation.

Several processes affect the chemical makeup of gas in a galaxy's ISM (inter-stellar medium). Galaxies accrete gas from the IGM (inter-galactic medium), stars in the galaxy can feed their mass back into the ISM in supernovae and stellar winds, and the galaxy can also lose gas in outflows. The feedback from stars is rich in heavy elements and is the means of enrichment of the ISM. On the other hand, the IGM is relatively poor in heavy elements,

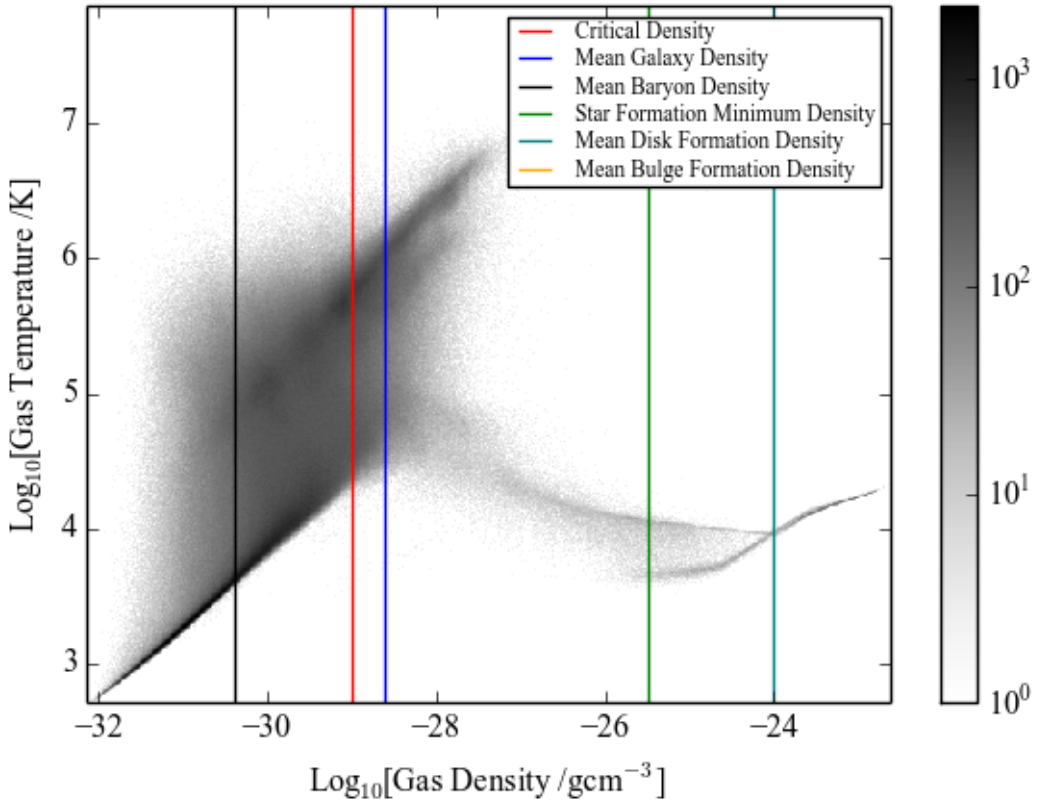

FIG. 3: A 2D histogram I created of temperature against density for every gas particle in the R12 simulation at snapshot 28 (z=0), with key densities marked using coloured lines. This demonstrates the effects of several of the subgrid models. For example, in the star forming region, we can see that a direct relationship is established, as star formation is modelled in the simulation using a subgrid model, a pressure dependent law with a metallicity threshold (Schaye & Dalla Vecchia 2008). The mean bulge formation density is not visible on the plot as it is off to the right.

and so accretion from the IGM dilutes the ISM. Galactic outflows can magnify these effects (M. C. Segers et al. 2016).

The various types of stellar feedback have characteristic element abundances, which can be used to trace the frequency of occurrence of those events from the chemical distribution of the ISM at various times. Of particular interest are core collapse supernovae and type Ia supernovae. Core collapse supernovae primarily eject α-elements, elements that are formed by progressive addition of α-particles, such as oxygen and magnesium. Type Ia supernovae occur with a characteristic delay relative to core collapse supernovae in a stellar population, and release mainly iron. As such, stellar populations formed earlier in a galaxy's history are expected to be "alpha enriched" compared those formed later, as there are more stellar populations which have evolved long enough to produce core collapse supernovae, but not type Ia supernovae (M. C. Segers et al. 2016).

In this report, square bracket notation is used to display element abundances. The relative abundance of elements A and B, $[A/B]$, in a sample is given as

$$[A/B] = Log_{10}(\frac{N_A}{N_B}) - Log_{10}(\frac{N_A}{N_B})_{\odot} \quad (1)$$

where N_A and N_B represent the abundances of element A and B in the sample respectively

2. METHODS

A repository of the python scripts written for this project is available on GitHub, from a link in the appendix.

A. Accessing the Data

The galaxy data were accessed from the EAGLE halo and galaxy catalogues SQL database (McAlpine et al. 2016) using the python module `eagleSqlTools` available from the project website (The EAGLE team 2017a). The particle data were accessed in hdf5 files available from The EAGLE team 2017a, using a modified version of the `read_eagle` routine from The EAGLE team 2017b. Galaxy data were used to identify galaxies in the simulation volume and filter them by mass, yielding the snapshot specific galaxy identifiers of group number and subgroup number, as well as the coordinates and velocity of the galaxy's centre of potential. Particle data by contrast were used to analyse the dynamics and characteristics of a particular galaxy, by reading the simulation's particle data and masking it to the group and subgroup numbers of the galaxy.

B. The Aperture Method

Before any analysis can be done on the bulge and disc and their formation, one must be able to identify the two components. The simplest method applied to this problem was to use a spherical aperture of radius 3 kpc around the centre of potential of a galaxy, separating the galaxy's star particles into two sets: those inside the aperture being defined as the bulge, and those outside it being defined as the disc.

This is useful as a computationally light way to probe the data, but clearly has serious shortcomings: that it will misclassify some bulge particles as disc particles and vice versa, and that it has no way to distinguish spiral galaxies from elliptical galaxies. Another shortcoming is that the aforementioned classification error does not affect all galaxies equally, as not all bulges are the same size. The 3 kpc aperture was chosen as a fair guide on the size of the bulge, as this method has no way to determine the size of the bulge.

C. The Circularity Method

A better way of approaching this problem is to use the metric of circularity. Circularity is essentially a measure of how well a particle's orbit aligns with the rotation of the galaxy. Circularity is defined as

$$\epsilon = \frac{L_{\parallel}}{L_c} \tag{2}$$

where ϵ represents the circularity of the particle, $L_{\parallel}$ represents the angular momentum of the particle in the direction of rotation of the galaxy, and L_c represents the angular momentum that the particle would have if it were on a circular orbit of the same specific energy as its current orbit. The circularity of a particle can vary from -1 to 1, as $|L_{\parallel}| \leq L_c$ since L_c is the highest possible angular momentum for an orbit of a given specific energy.

Circularity is an effective method for classifying galaxies and separating components because bulges and discs have different distributions of circularity. In a bulge, stars orbit in random directions, so the circularities should be distributed over the full interval, peaking at 0 and tapering off towards -1 and 1 due to an increased density of available orbits in directions perpendicular to the rotation of the galaxy relative to those parallel to it, and the eccentricity of orbits having a reductive effect on their circularity. In a disc however, stars orbit on near circular orbits in the galactic plane, in the direction of rotation of the galaxy, so their circularities should peak at 1. It is clearly not a perfect method, as there will still be some bulge particles with $\epsilon \simeq 1$ misclassified as disc particles, but this number will be very low in comparison to the aperture method.

To calculate ϵ for a particle one must first be able to calculate $L_{\parallel}$ and L_c.

1. Finding $L_{\parallel}$

$L_{\parallel}$ can be found by comparing the angular momentum of a particle around the galactic centre of potential, to the axis of rotation of the galaxy. The angular momentum, $\mathbf{L}$, of a particle is found as

$$\mathbf{L} = (\mathbf{r}_{particle} - \mathbf{r}_{gc}) \times \mathbf{v} \tag{3}$$

where m represents the mass of the particle, $\mathbf{r}_{particle}$ and $\mathbf{r}_{gc}$ represent the coordinates of the particle and the galaxy's centre of potential respectively, and $\mathbf{v}$ represents the peculiar velocity of the particle relative to the galactic centre.

Once $\mathbf{L}$ has been calculated for all the star particles in the galaxy, the rotation axis of the galaxy, $\hat{\mathbf{L}}_{stars}$, can simply be calculated as

$$\hat{\mathbf{L}}_{stars} = \frac{\Sigma\mathbf{L}}{|\Sigma\mathbf{L}|} \tag{4}$$

where $\Sigma\mathbf{L}$ is the sum of angular momenta of all star particles in the galaxy. Then $L_{\parallel}$ can simply be found as

$$L_{\parallel} = \mathbf{L} \cdot \hat{\mathbf{L}}_{stars}. \tag{5}$$

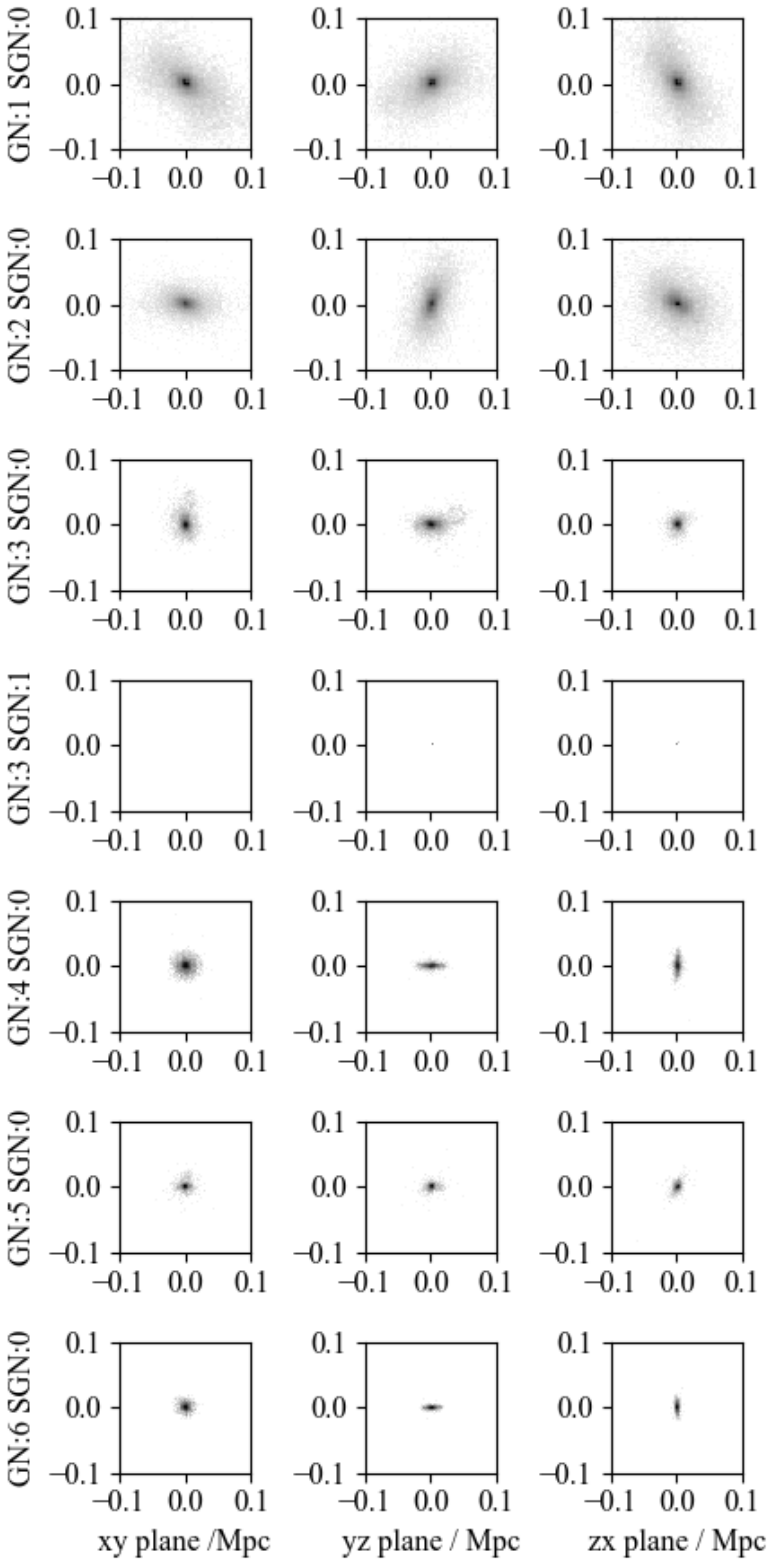

FIG. 4: 300x300 2D histograms of the spatial distribution of the stellar population of the 7 galaxies larger than $10^{10} M_{\odot}$ in the R12 simulation, in a rotated coordinate system that aligns their axes of rotation with the z axis. This figure displays the accuracy of my rotation axis calculations, as the galaxy discs are shown face on in the xy plane, and edge on in the yz and zx planes, as their rotation axes have been aligned to the z axis. The middle galaxy (GN:3 SGN:1) showing strange behaviour is a satellite galaxy, as indicated by its SGN of 1. This is likely due to an error in the `SUBFIND` algorithm.

2. *Finding L_c*

To find L_c, the specific energy of the particle's orbit must be found, and then used to find the angular momentum of a circular orbit with that specific energy. The specific energy of the orbit, E/m, is found as

$$\frac{E}{m} = \frac{1}{2}|\mathbf{v}|^2 + \phi \tag{6}$$

where $\mathbf{v}$ denotes the particle's velocity, and ϕ denotes the gravitational potential at the particle's coordinates. Once the specific energy of the orbit is known, it can be used to find L_c by establishing a relation between specific energy and angular momentum for radii from the galactic centre, and evaluating it for the specific energy in question.

This presents challenges that make L_c more difficult to calculate than $L_\parallel$. Firstly, ϕ is not included in the particle data, and so must be computed. To calculate ϕ for the location of a single particle requires one to compute and sum the contributions from every other particle in the galaxy of all types. This is computationally intensive. Secondly, the relation between the energies and angular momenta of circular orbits at a given radius must be ascertained. These problems can be solved with a variety of approximations of varying complexity of implementation, computational load, and accuracy, which are detailed below.

Note: For some of the other EAGLE simulations, binding energy is available in the particle data for dark matter, this would offer a much simpler way to find ϕ.

The simplest and least computationally intensive solution is to use the angular momentum of a circular orbit at the current radius of the particle as L_c. Unfortunately, this solution is also the least accurate. The solution works accurately for particles on circular or near-circular orbits, but is inaccurate for elliptical orbits, giving a much greater spread of circularity values, including ones that are outside the interval $-1 \leq \epsilon \leq 1$. This makes it more difficult to separate the bulge and disc particles. This is hereafter referred to as the 'same-radius' method.

A better solution is to use interpolation to calculate ϕ. In this method, a dataset of the masses of all particles in the galaxy, sorted by increasing radius from the galactic centre, is created. We then create a cumulatively summed version of the mass array, which tells us the mass enclosed by a sphere of the radius of each particle, this value will be hereafter referred to as the 'enclosed mass' of the particle. We then take a pre-determined number of interpolation points, distributed logarithmically in radius from the galactic centre. Increasing the number of interpolation points will improve the fit of the interpolation curve, but will also linearly increase the computational load of this step. We then compute ϕ at all the interpolation points, and polynomially interpolate to get a function that will give us an estimate of ϕ for any radius. We solve the second problem by computing the energies and angular momenta of circular orbits at specified radii using (3) and (6), with ϕ provided as above, and $\mathbf{v}_c$ given as

$$\mathbf{v}_c = \hat{\mathbf{L}}_{stars}\sqrt{\frac{GM(<r)}{r}} \tag{7}$$

where G denotes the gravitational constant, r denotes the radius from the galactic centre, and $M(<r)$ denotes the enclosed mass at that radius. For galaxies with a high number of particles, downsampling is also used to reduce the computational load. A randomly selected set of the

galaxy's particles is used to calculate the potential, and then this is multiplied by the mass of the galaxy over the mass of the sample. This is hereafter referred to as the 'interpolation' method.

Other solutions, not explored in this paper, include the shell model, which models the galaxy as spherically symmetric, so the enclosed mass can be used to estimate ϕ, fitting the potential to a Hernquist or NWF profile, and a tree code, which is the solution used by the EAGLE simulations. The shell model should lie somewhere between the same-radius and interpolation methods for both computational load and accuracy. The tree code would certainly be accurate, but far exceeds the other methods in complexity of implementation.

Once the circularity distribution of a galaxy has been computed, it can then be applied to categorise the galaxy, and to separate it into bulge and disc components. To categorise the galaxy, the disc and bulge mass fractions, w_d and w_b respectively, are calculated as

$$w_d = \frac{N_+ - N_-}{N} \qquad w_b = 1 - \frac{N_+ - N_-}{N} \tag{8}$$

where N represents the number of star particles in the galaxy, N_+ represents the number of those with positive circularity, and N_- represents the number with negative circularity. This works because the bulge is evenly distributed between positive and negative circularities, while the disc is only positive, so the numerator calculates the number of disc star particles.

Galaxies exist on a spectrum of bulge mass fraction. Ellipticals are at a fraction of $\sim$1 on one end, and the most discy spirals, like the Milky-way, are at $\sim$0.15 (Paul J. McMillan 2011) on the other end. Going from discy spirals to ellipticals we have galaxies with a shrinking disc fraction and a growing bulge fraction, until the disc entirely disappears. The cut-off point for what we consider a large-bulged spiral or an elliptical with a disc is somewhat arbitrary, and a disc/bulge fraction of 0.5 was chosen as the cut-off, as this represents the point where the disc becomes the dominant mass component.

Bulge mass fraction is not the only thing to be considered, peculiar galaxies are also a concern. If a galaxy has an asymmetric structure orbiting its centre of potential, the mass in that structure will be considered as disc mass in the above calculations, that is clearly not what is meant by a disc. In this paper, peculiar galaxies were filtered out visually, by inspecting images of the galaxies in R25, and histograms of the spatial distribution of stars in R12, as SKIRT images are not available for R12.

Visual inspection was a suitable method for filtering peculiar galaxies in this paper due to the relatively small number of galaxies considered (< 100), but would be unsuitable if these methods were extended to a larger sample. A more scalable method that doesn't require visual inspection is discussed in section *3. E. Further Work*.

Once a galaxy has been classified as a spiral, it is separated particle-wise into bulge and disc components. Particles with circularity $\epsilon < 0$ are classified as bulge particles, and those of $\epsilon > 0.85$ are classified as disc particles. This leaves particles of $0 < \epsilon < 0.85$ unclassified, as it is ambiguous whether they are bulge or disc particles. This should result in no disc particles misclassified as bulge, and only a very small number of bulge particles misclassified as disc. Using symmetry of the bulge to estimate the misclassification rate, it was found to be 0.8% $\pm$ 0.2% in spiral galaxies in R25. The misclassification rate can be visualised from Fig. 6, where the bulge particles misclassified as disc should be symmetric to what is shown with $\epsilon < -0.85$, which is clearly a tiny proportion of what is classified as disc ($\epsilon > 0.85$). This error

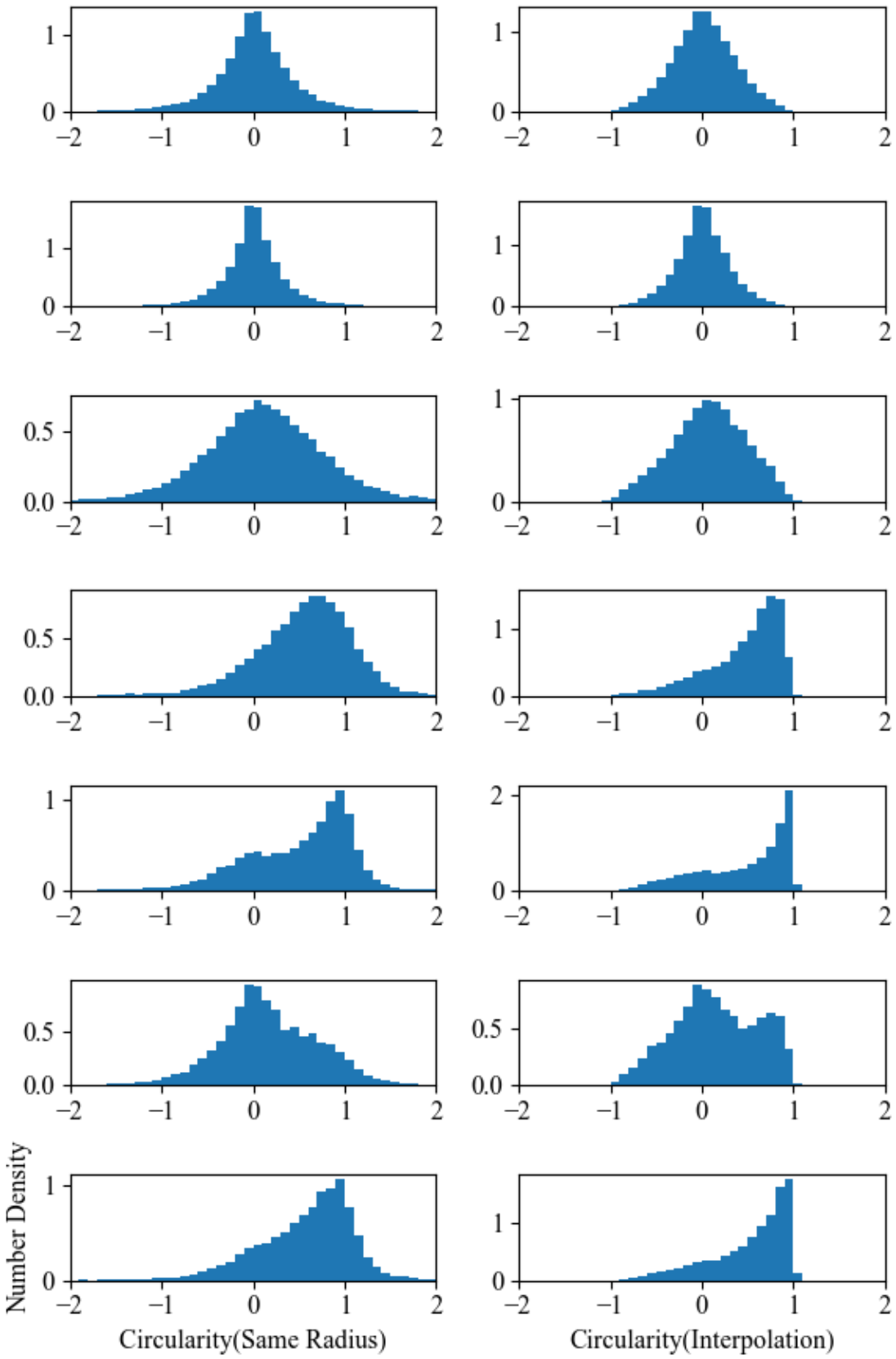

FIG. 5: A comparison of the same-radius and interpolation methods, as used to compute histograms of circularity for galaxies larger than $10^{10} M_{\odot}$. These are the same galaxies in the same order as shown in Fig. 4.

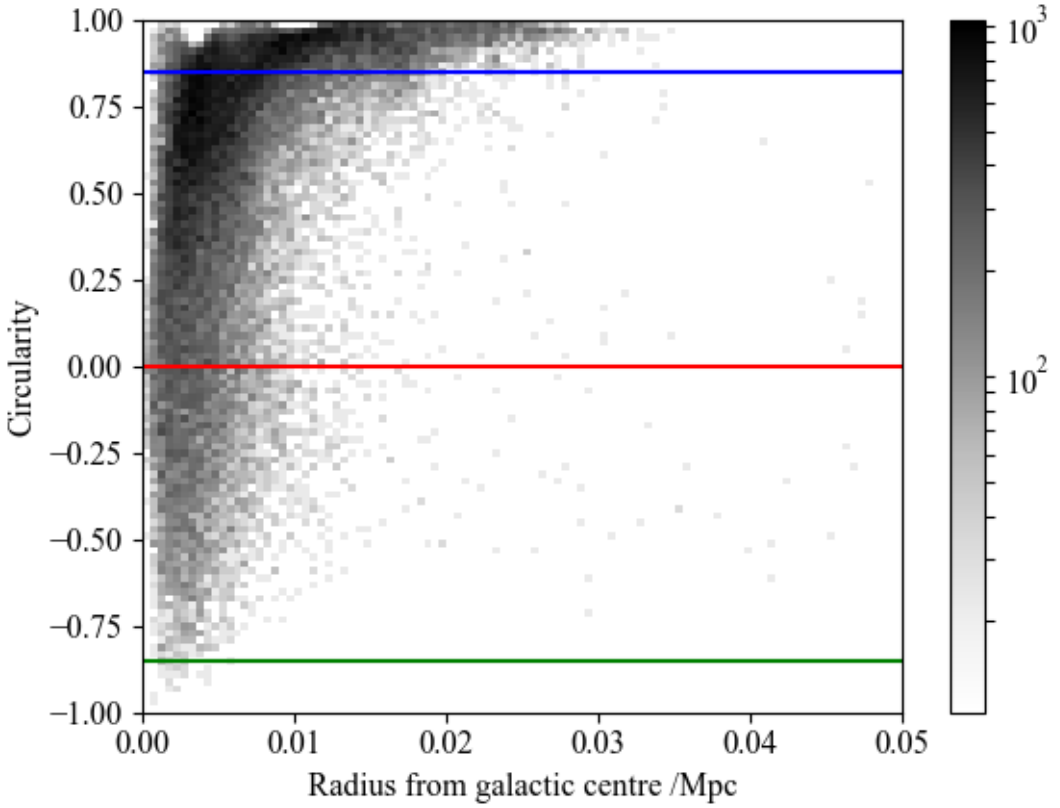

FIG. 6: A 100x100 2D histogram of circularity against radius for star particles in spiral galaxies in R12. The red marker shows the upper boundary for bulge classification, while the blue shows the lower boundary for disc classification. The green marker is a mirror of the blue. This figure intuitively displays how circularity can distinguish the components of a spiral galaxy. The scattering of points that can be seen at large radii are the stellar halo, the component symmetric around circularity 0 is the bulge, while the asymmetric component is the disc. The number of bulge particles misclassified as disc should be about even to those below the green marker, which is shown to be very small.

rate could be further reduced by imposing a radius limit, as the bulge particles cluster at much lower radius than the disc. This would be also result in a reduction of disc particles to analyse, though perhaps with a lower circularity cut-off and a radius cut-off, a lower error rate could be achieved at the same yield. Other properties of the particles, such as colour, age, or birth gas density could be used to get a better separation between the bulge and disc, but this is not done, as I seek to make inferences about the history of the particles using those properties, and these inferences would be void if I used those properties to make my classification.

The particle circularities are also stored in a hash table, with their particle IDs as keys for ease of later reference. These hash tables are included as .pickle files in the repository in the appendix.

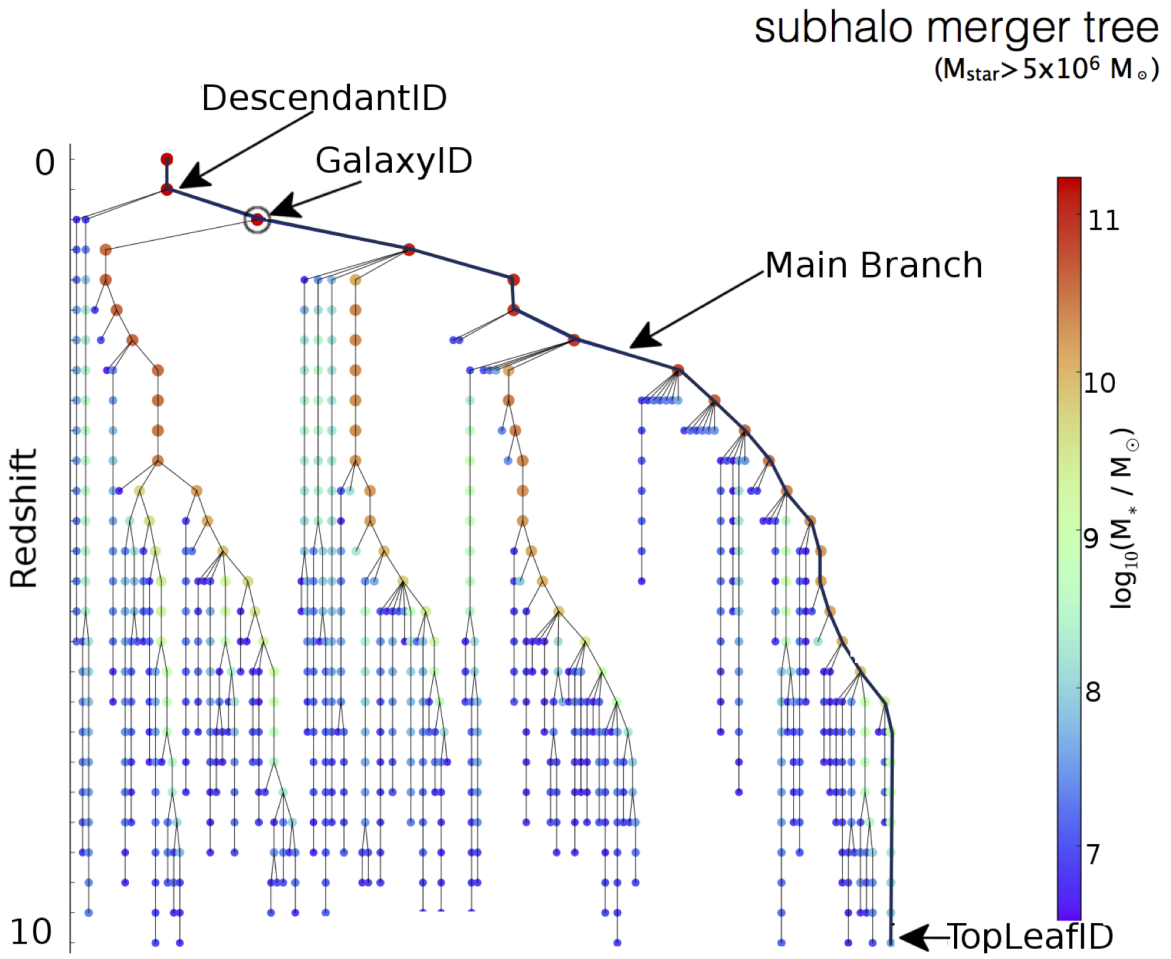

FIG. 7: An example merger tree (McAlpine et al. 2016). The present galaxy is shown at the top, with all its progenitors below it stacked by redshift. They are connected by mergers/accretions. The line shown in bold is the main progenitor line, which traces back from the present taking the highest mass progenitor to the main progenitor in the next snapshot.

D. Tracing Particles Histories Through the Merger Tree

Once the division of bulge and disc components has been performed, we can look at properties of the star particles in the bulge and disc separately, which gives some ability to look backward and investigate their origin through properties of their star particles, like their age, birth gas density, and feedback energy fraction.

To get a more comprehensive look at the history and formation of these components, one can trace a galaxy back through the snapshots and investigate how it has changed since its formation. The difficulty with this is that the galaxy identifiers in EAGLE are not persistent between snapshots, and furthermore it has to be clarified what is meant by ”tracing a galaxy back”, since galaxies continually accrete and merge with each other. This is addressed using a merger tree.

A merger tree exists for each galaxy in the final snapshot, and is a representation of its history, showing all of its progenitors and how they relate. An example of such a tree can be seen in Fig. 7. Information from these trees is available in the galaxy database.

To trace a galaxy back, all the star particle circularities are computed in its main branch descendants, and they are then linked by their particle IDs and plotted as tracks.

3. RESULTS AND DISCUSSION

A. The Aperture Method

Histograms of particle properties obtained using the aperture method are shown in Fig. 8(a), (b), and (c). The histograms of birth gas density and feedback energy fraction suggest a split in characteristics between bulge and disc stars, though the distributions of both the bulges and discs still appear bimodal. This is likely due to the misclassification of bulge and disc stars by the aperture method, which is illustrated by Fig. 8(d). In this 2D histogram we can see that there appear to be two separate peaks which might correspond to bulge and disc stars, but the aperture cuts through both of them, leaving a significant overlap. Worst of all, the birth expansion factor histogram does not show an expected clear split like the other two histograms.

B. The Circularity Method

Much better results are shown in Fig. 9. Here the bimodality is gone, and we see a much clearer distinction between the bulge and disc as expected. In the birth expansion factor histogram there is still a tail in bulge distribution to late times, and one in the disc distribution to early times. The disc tail could be a result of bulge particles being misclassified, but the bulge tail is certainly real. From these it can be seen that the bulge is formed in the early universe at high density, lending credence to the thought that the bulge is largely in place before the disc begins to form. The bulge tail could be caused by bar formation and destruction, but that mechanism cannot be the main source of the bulge, as most of the bulge forms before there is any disc to form a bar from, and the bulge forms at a much faster rate than this process could provide.

Further evidence of inside-out formation can be seen in Fig. 10 and Fig. 9(d). The bulge is clearly alpha-enriched compared to the disc, suggesting the bulge must have been in place before the disc formed around it. Fig. 10 also accurately reproduces observational evidence (T. Bensby et al. 2017), increasing confidence in the accuracy of the EAGLE simulations as a model of real galaxies.

C. Tracing Particle Histories

Figs. 11 and 12 give a view of the histories of particle circularities.

From the elliptical galaxy we can see sharp changes that initially have no clear cause. These are due to the fact that the elliptical galaxies have little to no net rotation, such that their axis of rotation is easily changed by small perturbations. Changes to the particles' circularities are predominantly due to small perturbations to the galaxy's angular momentum, rather than changes to the particles themselves. Unfortunately, this effect masks any other changes we might see to the particles, so all that can be determined from this is the lack of a disc.

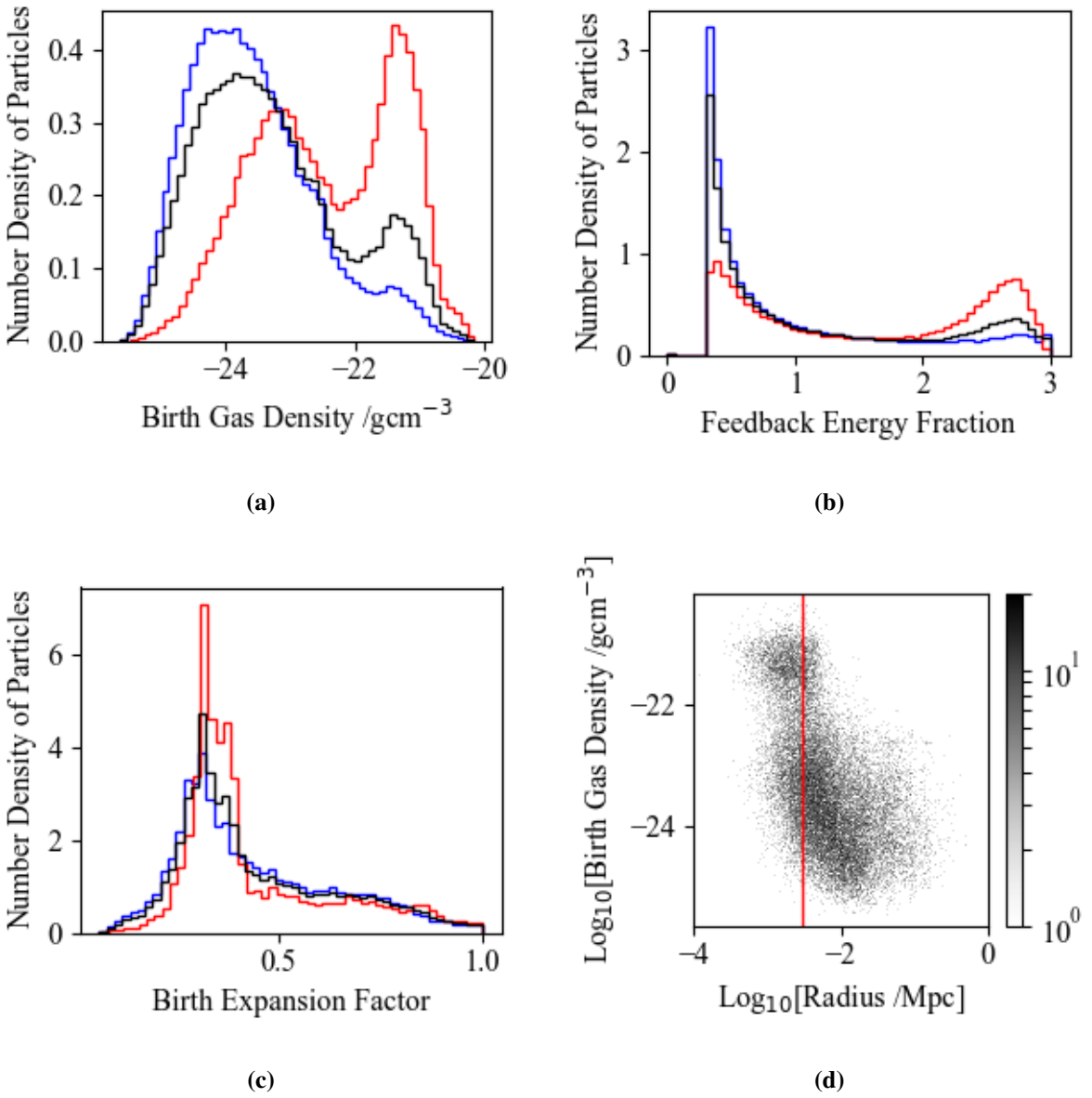

(a) **(b)**

(c) **(d)**

FIG. 8: Results from the aperture method. (a), (b), and (c) are normalised histograms of the birth gas density, feedback energy fraction, and birth expansion factor respectively of star particles in galaxies of stellar mass $> 10^{10} M_{\odot}$ in the R12 simulation. The black lines represent the total population of star particles, while the red lines represent the bulge particles, and the blue lines represent the disc particles. (d) is a 2D histogram of the birth gas density against distance from the galactic centre, with the red line showing the aperture radius.

In the spiral galaxy, we see the same obscurity before the disc forms. What we can see, however, is that by the time the disc forms, the bulge is already in place. If mergers were the primary mechanism for structure formation in spiral galaxies, we would expect to see large groups of bulge particles being born in a disc and undergoing a sudden transition together to the bulge. If bar formation and destruction was the primary mechanism, we would expect to see a more gradual and not tightly grouped transition of disc particles to bulge particles. Instead we

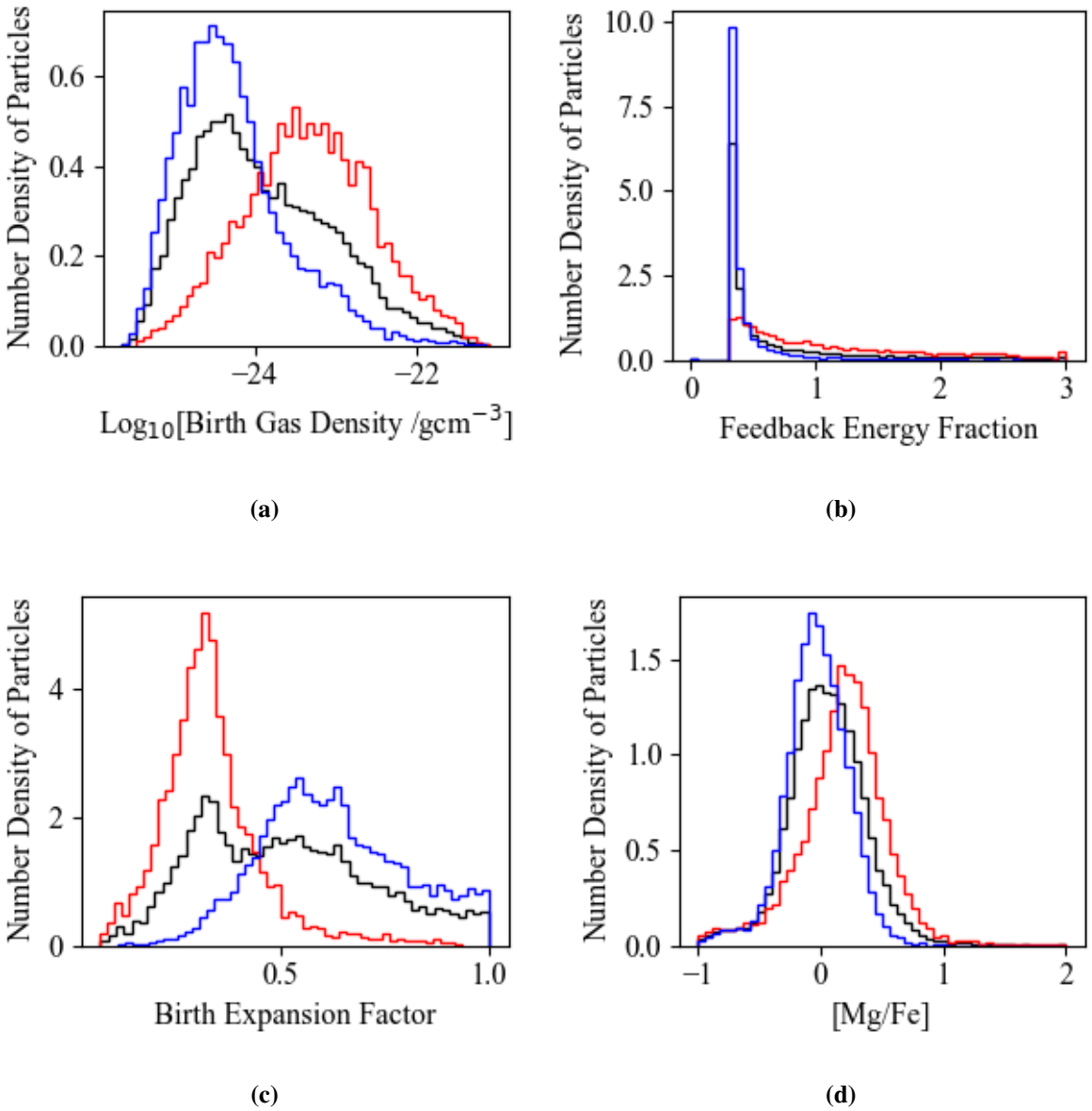

FIG. 9: Histogram results from the circularity method in R25. (a), (b), (c), and (d) are normalised histograms of the birth gas density, feedback energy fraction, birth expansion factor, and magnesium enrichment respectively of star particles in galaxies of stellar mass $> 10^{10} M_{\odot}$ in the R12 simulation. The black lines represent the total population of star particles, while the red lines represent the bulge particles, and the blue lines represent the disc particles. A more comprehensive look at alpha enrichment is shown in Fig. 10.

see that disc particles broadly remain in the disc, and the bulge particles are almost all formed and already in the bulge before the disc appears. These results are limited to only two galaxies due to computational restraints, limiting confidence in the conclusions they reach, but we can still discount mergers and bar formation/destruction as the main or only mechanisms of spiral galaxy structure formation.

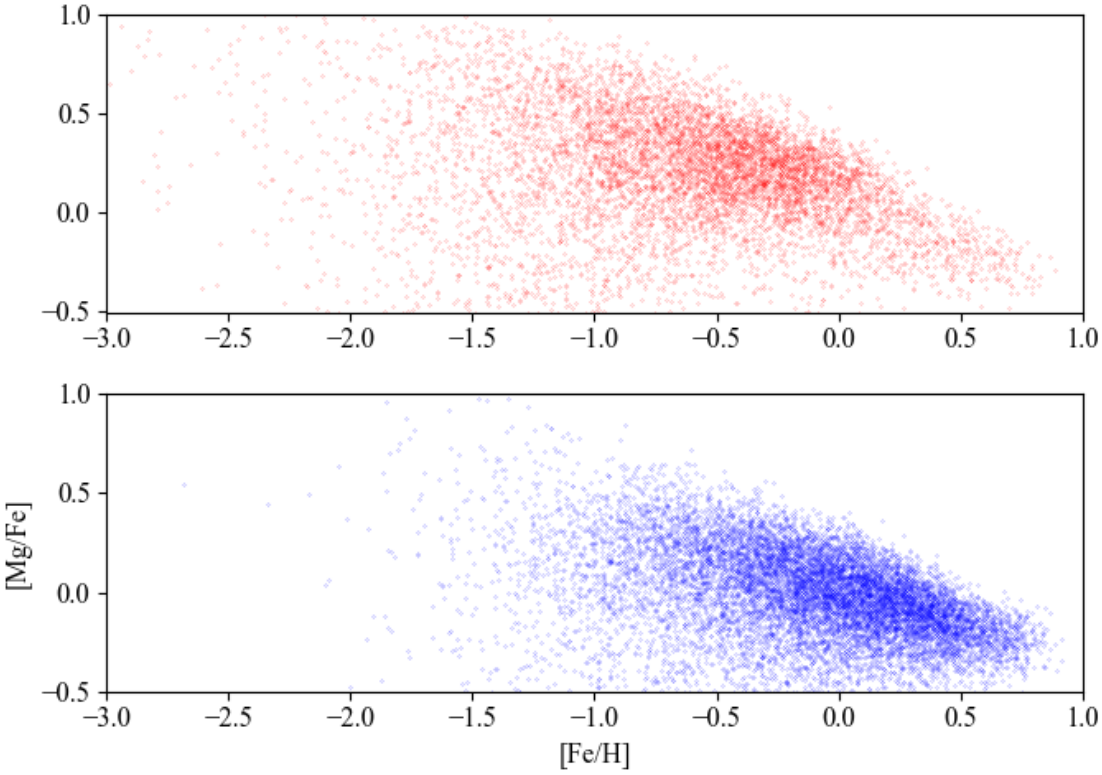

(a)

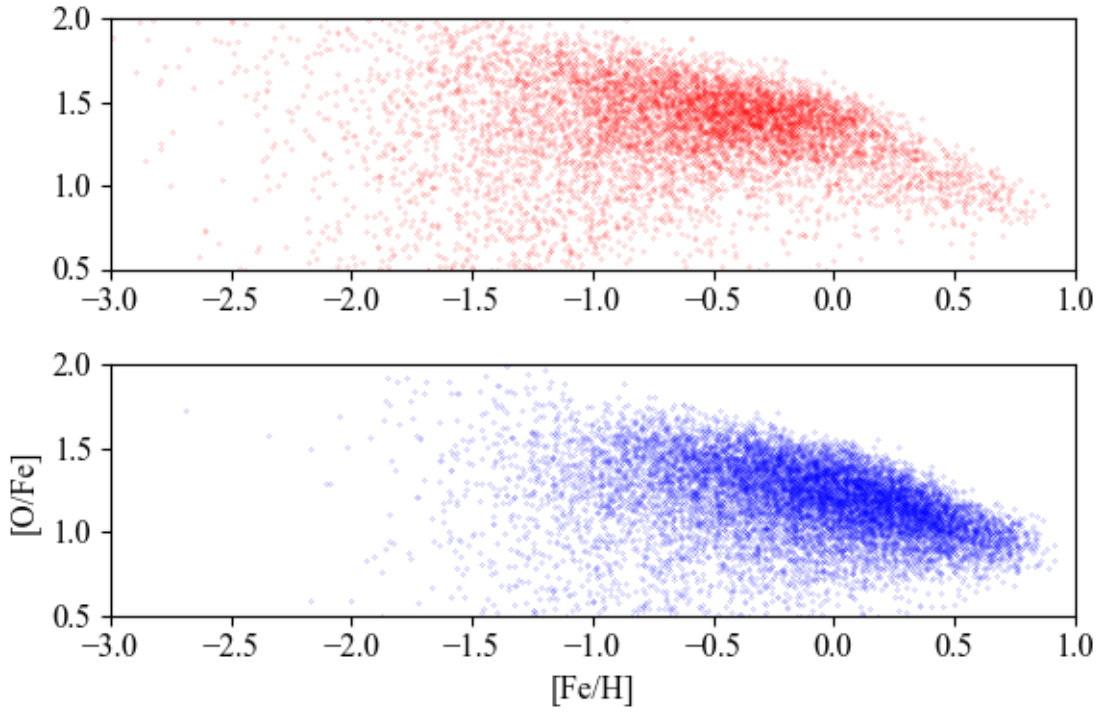

(b)

FIG. 10: Plots displaying alpha enrichment (oxygen and magnesium) for the bulges (red) and discs (blue) separately. Solar metallicity values are taken from R. Wiersma et al. 2009.

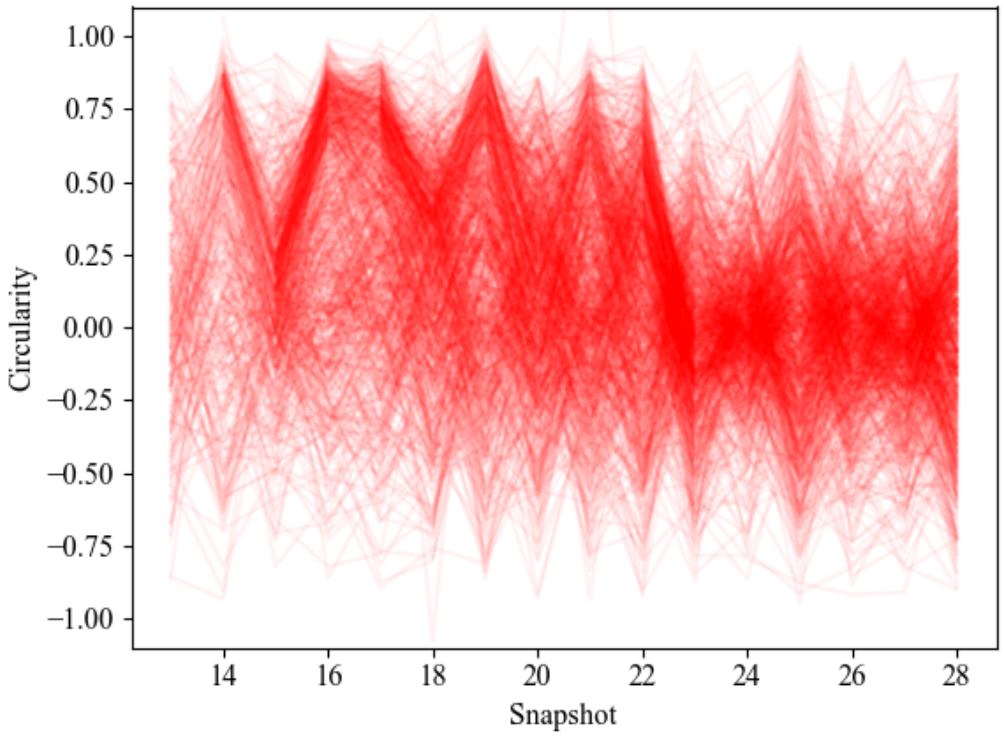

(a) Elliptical

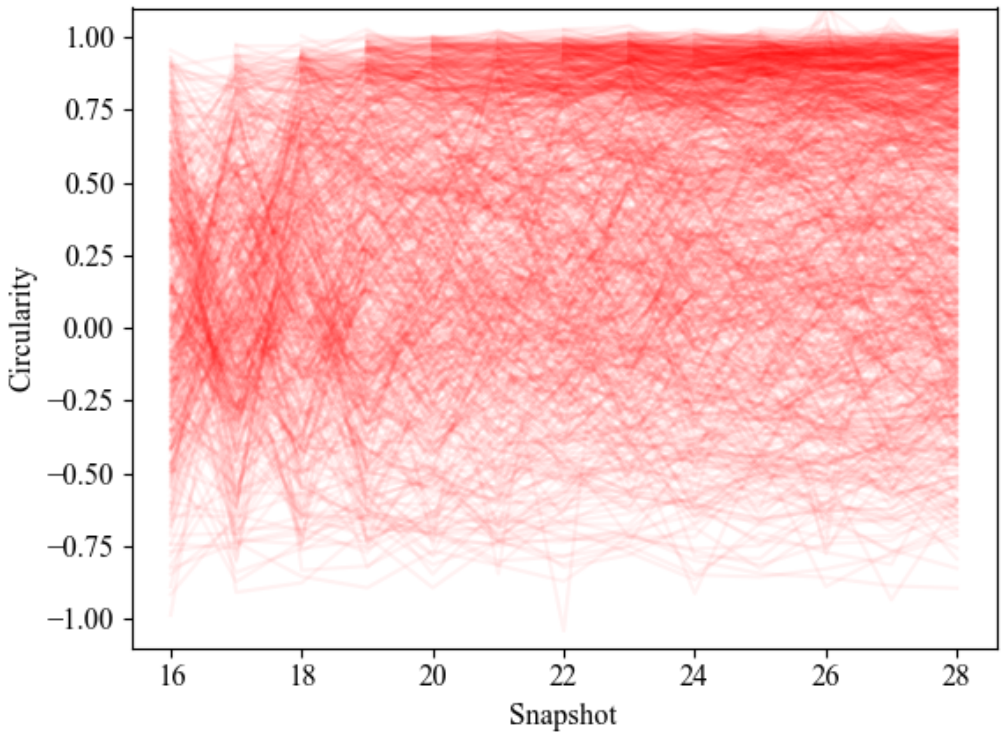

(b) Spiral

FIG. 11: Kinematic histories of the largest Elliptical and Spiral Galaxies in R12. The elliptical is shown in (a), and the spiral in (b). The histories are downsampled to 1000 randomly chosen particles for readability.

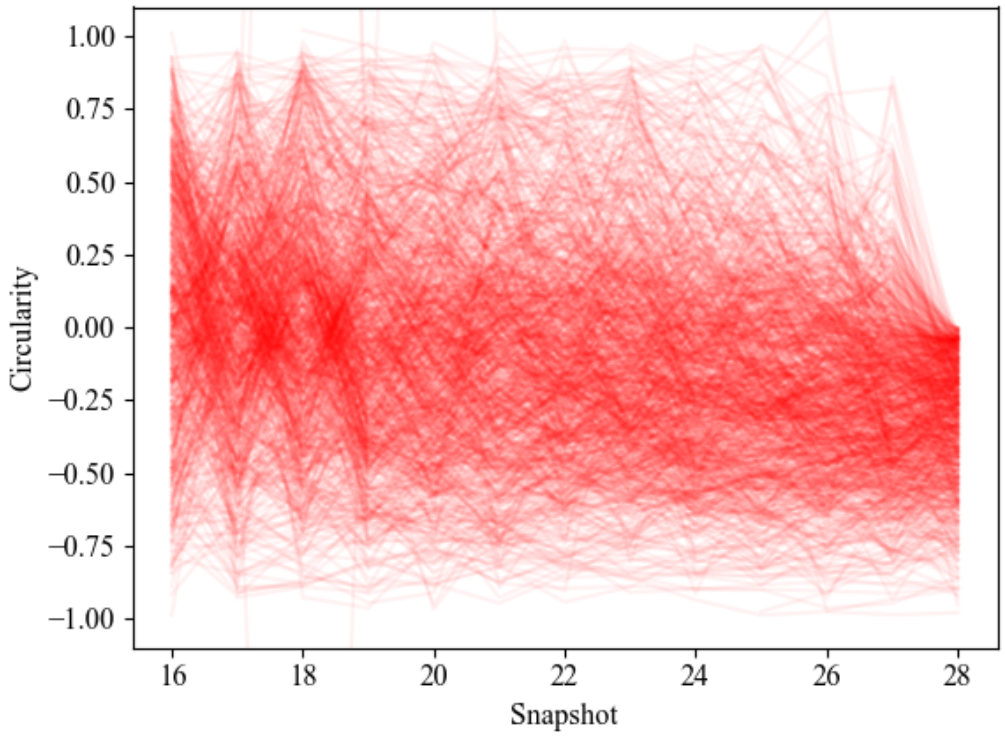

(a) Bulge

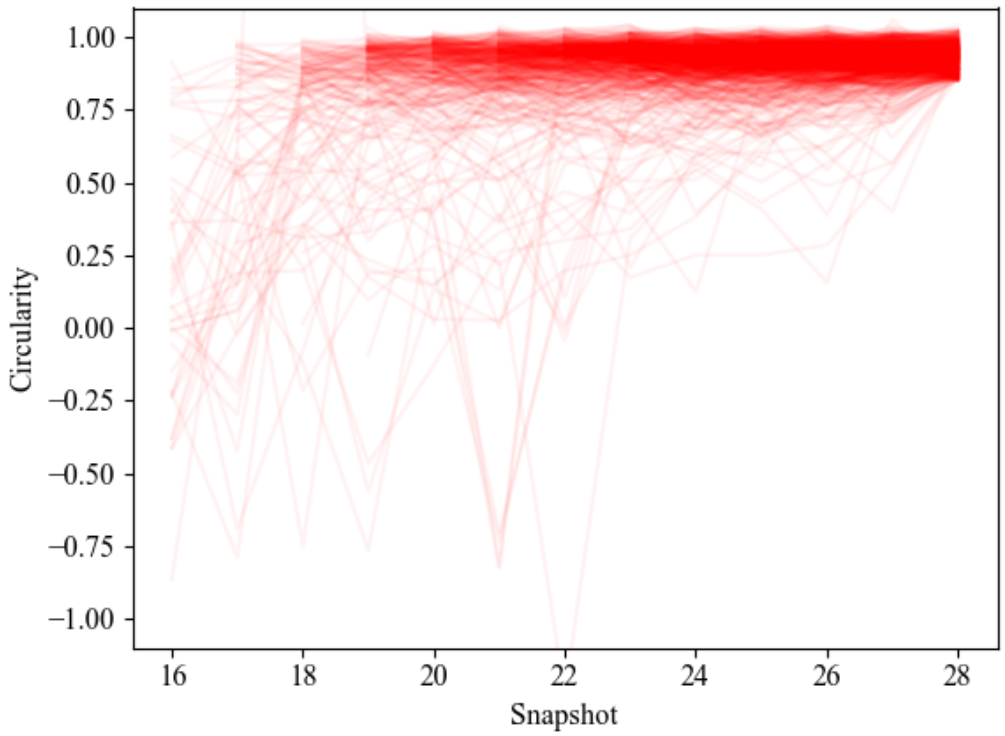

(b) Disc

FIG. 12: Kinematic histories of the bulge and disc of the largest spiral galaxy in R12. The bulge is shown in (a), and the disc in (b). The histories are downsampled to 1000 randomly chosen particles for readability. The low circularity scatter in the (b) is due to bulge particles being misclassified as disc.

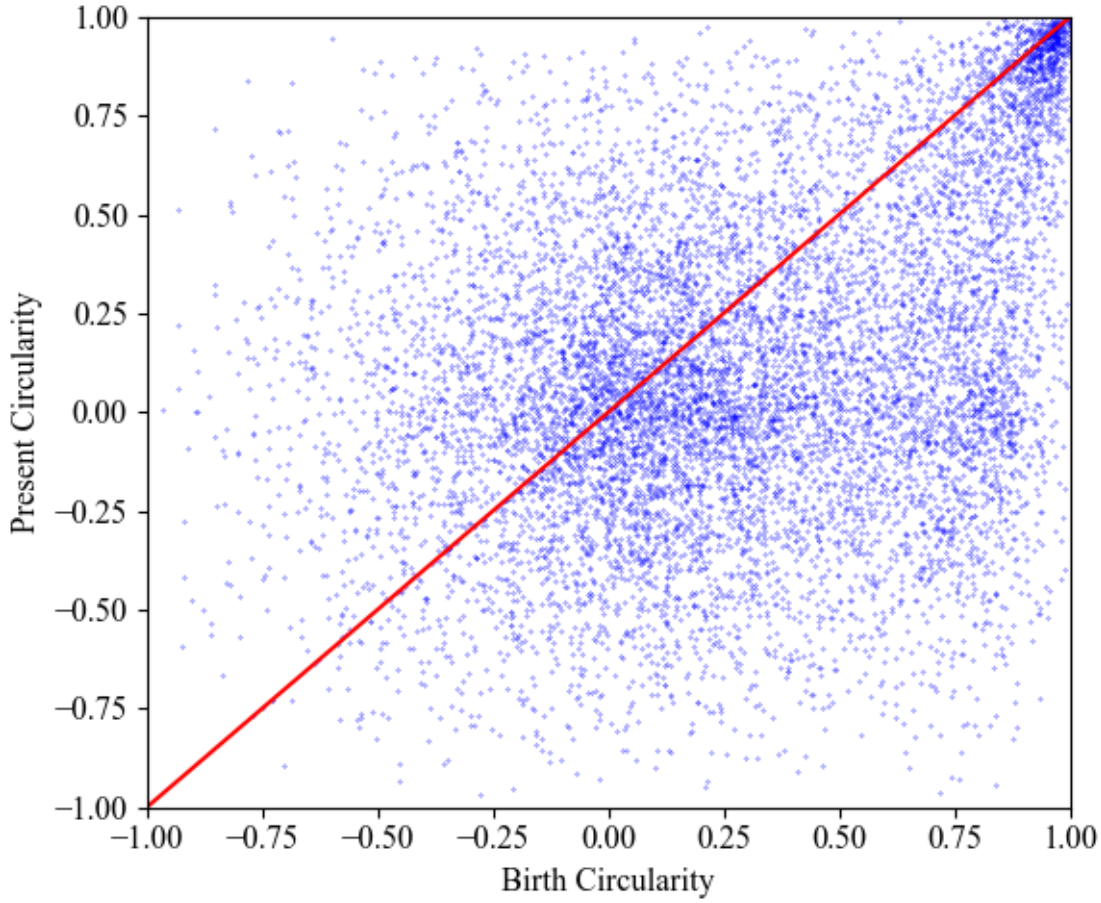

FIG. 13: Plot of the circularities of particles in spiral galaxies in R12 when they were born against their circularities at present. The red line indicates where they are the same.

D. Lifetime Changes

In Fig. 13 we can see the relation between particle circularities at birth vs. at present.

Apart for the smudged cluster on the right of the graph, the distribution of particles is roughly symmetric about the $x = 0$ and $y = 0$ lines, this symmetric background represents the bulge that is in place before the disc forms.

The smudge shows particles that formed in the disc. We can clearly see that disc particles are all born in the disc. This makes sense, as we know that the disc contains star forming gas, and there is no known or proposed process that could convert bulge stars to disc.

However, we do see the reverse happening, disc particles turning into bulge particles. Though it is clear from this plot that this is not the main process of bulge formation, just a minor contributor. This could be due to gravitational interactions with other objects such as bulge and halo stars, bar formation and destruction, or a combination of the two.

E. Further Work

The data analysis in this work was heavily limited by computing resources, as the data were processed on mid-range consumer hardware. The primary limiting factors were storage and network bandwidth. Storage was not available for optimisation since it was predefined by the size of the EAGLE particle data files, and the EAGLE files had to be downloaded from the online repository. Processing power and memory usage, on the other hand, were well optimised for in the code.

The limitations of storage and bandwidth resulted in a limit on available simulation volume. Full specification analysis was only performed on the R12 simulation, and single snapshot analysis on the R25 simulation. The limitation in simulation volume resulted in a limitation in available galaxies for analysis, with 3 spiral galaxies of mass $> 10^{10} M_{\odot}$ in the R12 simulation, and 25 galaxies in the R25.

Future work to extend the analysis to a larger population of galaxies would simply be a matter of running the code on a larger volume simulation. It could also be done with higher resolution simulations. This would give more representative results, with more opportunity to investigate edge cases, and would also increase confidence in the results obtained. Such an extension would only require better storage capacity (15 TB for the 100 Mpc simulation) and easier access to the particle data, as downloading 15 TB on a consumer internet connection is infeasible.

Extending to larger simulations would also allow the use of SKIRT images of the galaxies to compare with their kinematic histories. The code is already written to do this, but the SKIRT images are unfortunately not available for R12.

Another possible extension, if using a larger simulation volume, would be to investigate bar formation and destruction in more depth, perhaps by searching for a correlation between bar size and the conversion of disc mass into bulge.

In terms of run time, the R12 simulation data processed in $\sim$30 minutes on a netbook with a heavily underclocked CPU. As run time scales roughly with simulation volume, we could expect a runtime of $\sim$30 hours for the 100 Mpc simulation on the same processor. This is already a reasonable run time, and it would see improvements of more than an order of magnitude with a more powerful CPU.

Running on larger simulations would greatly benefit from automated classification of peculiar galaxies. This could be done by drawing planes at a range of angles through the galaxy centre, and comparing the mass on either side. Large mass inequalities would indicate asymmetry in that plane, signalling that a galaxy is peculiar.

The algorithms developed in this project could also be easily ported to investigate other simulations and compare their results. Most of the functions could even be used unchanged, the only large change that would be needed would be an appropriate replacement of the `read_eagle` routine to extract data, and a pre-processor to format the data ready for input to the other functions.

4. CONCLUSIONS

In conclusion, I present an investigation of spiral galaxy formation in the EAGLE cosmological simulations, by means of tracing the kinematics of stars in galaxies through their formation, as well as investigating the properties of age, birth gas density, feedback energy fraction, and element abundances in the bulge and disc components of the galaxies. These all point to the bulge being largely in place before the disc begins to form, and also offer evidence of a lesser process that converts disc into bulge, consistent with conclusions from recent observational studies.

Acknowledgments

The author would like to thank Professor Tom Theuns for his supervision and support over the course of the project.

References

[E. Bell et al. 2001] E. Bell et al. The Accretion Origin Of The Milky Ways Stellar Halo, The Astrophysical Journal, 548, 33-46 (2001)

[Freedman & Diaconis 1981] D. Freedman and P. Diaconis, "On the histogram as a density estimator: L2 theory", Probability Theory and Related Fields. Heidelberg: Springer Berlin. 57 (4), 453476 (1981)

[Gnedin et al. 2000] N. Gnedin et al. Formation of Galactic Bulges, The Astrophysical Journal, 540, 32-38 (2000)

[Hopkins et al. 2010] P. Hopkins et al. Discriminating between the physical processes that drive spheroid size evolution, MNRAS, 401 issue 2, 1099-1117 (2010)

[K. Dolag et al. 2009] K. Dolag et al. Substructures in hydrodynamical cluster simulations, Monthly Notices of the Royal Astronomical Society 399, 497514 (2009)

[Kauffmann et al. 1996] G. Kauffmann et al. Detection of Strong Evolution in the Population of Early-Type Galaxies, MNRAS, 283 issue 4, 117-122 (1996)

[M. C. Segers et al. 2016] M. C. Segers et al. The origin of the -enhancement of massive galaxies, Monthly Notices of the Royal Astronomical Society, Volume 461, 102-106 (2016)

[M. Davis et al. 1985] M. Davis et al. The Evolution of Large Scale Structure in a Universe Dominated by Cold Dark Matter, The Astrophysical Journal, 292, 374-391 (1985)

[Margalef-Bentabol et al. 2016] B. Margalef-Bentabol et al. The Formation of Bulges, Discs and Two Component Galaxies in the CANDELS Survey at z<3. Monthly Notices of the Royal Astronomical Society, 461. . (2016)

[Margalef-Bentabol et al. 2017] B. Margalef-Bentabol et al. Stellar populations, stellar masses and the formation of galaxy bulges and discs at z<3 in CANDELS, Monthly Notices of the Royal Astronomical Society, Volume 473, Issue 4, p.5370-5384 (2017)

[McAlpine et al. 2016] S. McAlpine et al. The eagle simulations of galaxy formation: public release of halo and galaxy catalogues, Astronomy and Computing, 15, 72-89 (2016)

[N. Grogin et al. 2011] N. Grogin et al. CANDELS: The Cosmic Assembly Near-infrared Deep Extragalactic Legacy Survey, The Astrophysical Journal Supplement Series (2011)

[O.M. Kurth et al. 1999] O.M. Kurth, U. Fritze, V. Alvensleben, and K.J. Fricke. Evolutionary synthesis of simple stellar populations - Colours and indices, Astronomy and Astrophysics Supplementary Series Volume 138, Number 1 (1999)

[Paul J. McMillan 2011] Paul J. McMillan. Mass models of the Milky Way, Monthly Notices of the Royal Astronomical Society, Volume 414, Issue 3, 24462457 (2011)

[R. Wiersma et al. 2009] R. Wiersma et al. Chemical enrichment in cosmological, smoothed particle hydrodynamics simulations, Monthly Notices of the Royal Astronomical Society 399, 574-600 (2009)

[Schaye & Dalla Vecchia 2008] Schaye & Dalla Vecchia, On the relation between the Schmidt and KennicuttSchmidt star formation laws and its implications for numerical simulations, Monthly Notices of the Royal Astronomical Society, Volume 383, Issue 3, 12101222 (2008)

[Schaye et al. 2015] J. Schaye et al. The EAGLE project: simulating the evolution and assembly of galaxies and their environments, Monthly Notices of the Royal Astronomical Society, 446, 521554

(2015)

[Sellwood et al. 2004] J. Sellwood et al. The Destruction of Bars by Central Mass Concentrations, The Astrophysical Journal, 604, 614-631 (2004)

[Springel 2005] V. Springel, The cosmological simulation code GADGET-2, Monthly Notices of the Royal Astronomical Society, 364, 11051134 (2005)

[T. Bensby et al. 2017] T. Bensby et al. Chemical evolution of the Galactic bulge as traced by microlensed dwarf and subgiant stars - VI. Age and abundance structure of the stellar populations in the central sub-kpc of the Milky Way, Astronomy & Astrophysics 605, A89 (2017)

[The EAGLE team 2017a] The EAGLE team, The EAGLE project public data, http://icc.dur.ac.uk/Eagle/database.php (2017)

[The EAGLE team 2017b] The EAGLE team, The EAGLE simulations of galaxy formation: Public release of particle data, arXiv:1706.09899 (2017)

[Verstocken et al. 2017] Verstocken et al. SKIRT: Hybrid parallelization of radiative transfer simulations, Astronomy and Computing, Volume 20, 16-33 (2017)

[Wendland 1995] H.Wendland, Piecewise polynomial, positive definite and compactly supported radial functions of minimal degree, Adv. Comput. Math. 4, 389396 (1995)

5. APPENDIX

Python scripts developed for this project can be found at:
https://github.com/inTarga/L4Project